10452 *Macromolecules* **2010**, *43*, 10452–10456
DOI: 10.1021/ma101883w

Macromolecules
ARTICLE

Directed Assembly of Nanoparticles in Block Copolymer Thin Films: Role of Defects

Jenny Kim and Peter F. Green*

Department of Materials Science and Engineering and Department of Chemical Engineering, Applied Physics, University of Michigan, Ann Arbor, Michigan 48109, United States

Received August 16, 2010; Revised Manuscript Received November 10, 2010

ABSTRACT: The structure of A-*b*-B diblock copolymer (BCP) thin films is often exploited for "tailoring" the self-assembly of nanoparticles into various geometries, characterized by long-range order. Mechanistically, the nanoparticles are sequestered within the A or B domains of the copolymer, and the domains act as scaffolds to direct the assembly of the nanoparticles. We show that in BCP thin films, which order at suboptimal thicknesses, dislocations play a dominant role in determining the spatial organization of sufficiently large nanoparticles. The nanoparticles preferentially segregate to the core of edge dislocations, which are ubiquitous in these materials. To this end, the two-dimensional planar shape of the islands and holes determine the self-assembled geometry of the nanoparticles. We also show that the so-called "healing length", λ, increases with film thickness, h, in a manner consistent with $\lambda \propto h^{1/2}$, in accordance with theory. In films of thickness between $L < h < 3L$, where L is the domain spacing, λ largely determines the average size of the region within which the nanoparticles are sequestered.

Introduction

Functional materials that rely on the combined properties of soft materials and the functionality of inorganic nanoparticles comprise a technologically important class of materials, polymer nanocomposites (PNCs).[1−4] The use of phase-separated A-*b*-B diblock copolymers as scaffolds enables self-organization of the nanoparticles (NPs) into patterns characterized by long-range order.[5,6] The self-assembled nanoparticle pattern is dictated by the BCP domain symmetry because the nanoparticles are confined within the domain with which their interactions are thermodynamically most favorable.

The distribution of spherical nanoparticles, of diameter d, within a BCP which possesses a lamellar morphology, for example, is generally determined by the ratio d/L, where L is the interlamellar thickness. Monodisperse particles of sufficiently small d/L, typically $d/L < 0.15$, would be located throughout the appropriate domains, thereby maximizing the translational entropy. The chains would stretch, costing entropic (elastic) energy, in order to accommodate nanoparticles; the gain in translational entropy of the nanoparticles offsets this cost in entropic energy.[7,12−15] Since the nanoparticles are located throughout a given domain, including at the A/B boundaries, the number of unfavorable A/B contacts is reduced; this has the effect of reducing the interfacial tension. Under these conditions, the system is less stable toward order−order and order−disorder transitions.[7−11] However, then d/L increases the entropic penalty due to chain stretching becoming significant, and the nanoparticles become more localized toward the center of the appropriate domains, away from the A/B interfaces.

It has been shown that the lateral distribution of nanoparticles within the domains of the BCP/NP system can be quite sensitive to size distributions of nanoparticles. The larger particles reside preferentially toward the center of the domains, whereas the smaller nanoparticles are preferentially distributed toward the boundaries.[7,16−18] Nanoparticles are also known to segregate to defects, such as dislocations and grain boundaries, which are well-known to exist in bulk BCPs.[19,20] Typically, the NPs preferentially segregate to high angle grain boundaries.[21−23] At sufficiently large volume fractions nanoparticles may form separate phases.[12]

Nanoparticles have been shown to form nanoscale periodic structures, exhibiting long-range order, within the phase-separated domains of thin film BCPs on chemically or topographically patterned substrate.[24−26] Of particular interest in this paper is the organization, self-assembly, of brush-coated nanoparticles in A-*b*-B diblck copolymer thin film hosts. By way of context we note that islands and holes reside at the surface of BCP thin films of suboptimal thicknesses in the phase-separated, ordered, state. They comprise the excess material at the free surface, not contributing to the formation of a complete layer.[10,11,27−29] Because edge dislocations enable the transition between the complete layer and the islands and holes, they are ubiquitous in thin BCP films.

We show that in thin BCP films edge dislocations play a prominent role in the self-organization of nanoparticles when d/L is sufficiently large. When d/L is sufficiently small, the nanoparticles reside predominantly within the domains. However, when d/L is sufficiently large, the nanoparticles preferentially reside at the core of edge dislocations in thin films. Therefore, the long-range self-assembled nanoparticle patterns manifest the two-dimensional, planar, circular, patterns of the islands/holes. The nanoparticles are not uniformly distributed along the dislocation cores and instead form clusters, with nearly periodic spacing.

Experimental Section

Gold nanoparticles (Au NPs) were synthesized using the two-phase arrested precipitation method reported by Brust et al.[30] Thiol-terminated polystyrene molecules (PS-SH) of number-average molecular weight $M_n = 1000$ g/mol ($M_w/M_n = 1.4$), purchased from Polymer Source, Inc., were then grafted onto the surfaces of the nanoparticles. The details of our synthetic procedures are described in earlier publications.[31−33]

*To whom correspondence should be addressed.

 Published on Web 11/29/2010 © 2010 American Chemical Society

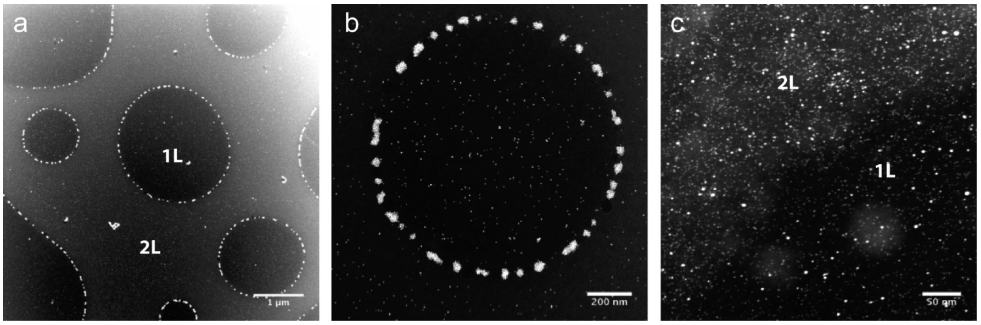

Figure 1. STEM images of the lateral distribution of nanoparticles in BCP thin films of thicknesses in the range $3L/2 < h < 2L$, containing 3 wt % nanoparticles. (a) The image of a film containing NPs of average diameter 5.1 nm is shown; the holes are of height $h = L$ above the substrate, and the adjacent layer is of height $h = 2L$. (b) A magnified image of (a). (c) The edge of a hole in a film containing NPs of average diameter 1.8 nm. Layers of height $h = L$ and $h = 2L$ are identified in the image.

The diameters of the NP cores, d_{core}, and the brush thicknesses, h_{brush}, were determined from scanning transmission electron microscopy (STEM) images of the samples, obtained using a JEOL 2010F electron microscope operated at 200 kV. The average particle sizes were determined by measuring the diameters of groups more than 300 NPs in the images. Two sets of grafted nanoparticles were prepared: (1) Au(5)-PS is a nanoparticle of $d_{core} = 5.1 \pm 1.2$ nm and $d_{NP} = d_{core} + 2h_{brush} = 8.9 \pm 1.1$ nm; the average degree polymerization of the grafted chains is $N = 10$ of the chain grafting density is $\sigma = 2.1$ chains/nm^2; (2) Au(2)-PS is a nanoparticle of $d_{core} = 1.8 \pm 0.5$ nm; $d_{NP} = 4.5 \pm 1.1$ nm, $N = 10$ and $\sigma = 1.4$ chains/nm^2.

Poly(styrene-*b*-*n*-butyl methacrylate) (PS-*b*-PnBMA) diblock copolymers of number-average molecular weight $M_n = 86\,700$ g/mol and dispersion $M_w/M_n = 1.08$ were purchased from Polymer Source, Inc. The M_ns of the PS and the PnBMA blocks were 43 700 and 43 000 g/mol, respectively, and the volume fraction of PS block was $f_{ps} = 0.58$. This system exhibits a lamellar morphology.

Homogeneous solutions containing well-defined concentrations of the copolymer and the nanoparticles were prepared using toluene as a solvent. The solutions of PS-*b*-PnBMA/Au(d_{NP})PS$_N$ ($N = 10$) mixtures were spin-cast onto silicon nitride (Si_3N_4)-coated silicon substrates; the Si_3N_4 layer of thickness 100 nm was grown by LPCVD (WaferNet, Inc.). The initial film thicknesses, h_0, of the nanocomposite samples were determined using spectroscopic ellipsometry.

The morphologies of the BCP thin films, the Au NP distributions and the topographies of the sample were determined using a combination of scanning force microscope (SFM) and STEM. The samples examined using STEM were prepared first by spin-casting their solutions onto a glass slide and then floating the film from the slide onto a bath of distilled water. The films were then transferred onto a Si_3N_4 grid and subsequently dried by annealing them in vacuum at 60 °C for 16 h. Finally, prior to STEM and SFM analysis, the samples were subjected to supercritical carbon dioxide (sc-CO_2) annealing at a temperature of $T = 60$ °C and a pressure of $P = 13.8 \pm 0.3$ MPa for durations of time between 2 and 72 h. sc-CO_2 was used because it is a poor solvent; it plasticizes the films. The temperature and the pressure determine the extent of swelling that a film would undergo. We are able to control the swelling of the samples in sc-CO_2 environments much better than in toluene vapor, where we made similar observations regarding the particle segregation. In-situ spectroscopic ellipsometry was used to monitor the changes in film thickness in order to ensure control of the film thicknesses under the processing environments. Additional details of the annealing procedure are described elsewhere.[31]

Some of the samples that underwent sc-CO_2 annealing were also subjected to ruthenium tetraoxide (RuO_4) vapor for 5−10 min and then examined using STEM. RuO_4 selectively stains the PS phase so it could become apparent in the images when necessary. Image J software was used to analyze the STEM images. Specifically, the average cluster size $R(t)$ was determined by analyzing projected surface area in STEM image using Image J software.

We note that when these materials were annealed under vacuum conditions; above the glass transition, there was clear evidence of segregation of the nanoparticles to the dislocation cores. However, after a few hours, the nanoparticles begin to coarsen, as the ligands became detached. Therefore, we did not rely on high-temperature annealing under vacuum.

SFM measurements of the films were performed using the MFP-3D (Asylum Research, Inc.) microscope, in tapping (AC) mode. Silicon cantilevers (Olympus, Inc.), each with a spring constant of 42 N/m and resonant frequency of 300 kHz, were used. The SFM images were analyzed using Igor Pro (Asylum Research, Inc.) software.

The interlamellar spacings, L, of the films are readily determined using SFM by taking advantage of the fact that diblock copolymer films, and droplets, form steps when in contact with the substrate. The steps are readily observed after scratching the film, thereby exposing the underlying substrate, and annealing. The step heights provide a measure of the interlamellar spacings of the phase-separated system. The edges of PS-*b*-PnBMA form steps on Si_3N_4 and on SiO_x, substrates upon annealing in vacuum and/or in sc-CO_2. The step heights determined, using SFM, from samples annealed in vacuum at 150 °C were 30 ± 2 nm, and they were 33 ± 2 nm for samples annealed in CO_2 at 60 °C.[34] Our data are in agreement with published data on this system.[35]

Results and Discussion

We begin by noting that the PS-*b*-PnBMA copolymer orders symmetrically on the substrates, wherein PnBMA resides at the substrate and at the free surface. The surface energy of PnBMA is less than that of PS, and it is more polar, which explains the wetting behavior of the material. The lateral distributions of nanoparticles throughout films of thicknesses $1.6L < h < 2L$ are sensitive to the nanoparticle sizes, as illustrated by the STEM images in Figure 1. The STEM image in Figure 1a is that of a film containing 3 wt % of the Au(5)-PS nanoparticles. The darker regions, within the circular nanoparticle patterns, of the image are holes of depth L below the free surface. The lighter regions are thicker regions of $h = 2L$. Shown in Figure 1b is a magnified image, which includes a hole. It is apparent from this image that while nanoparticles preferentially reside at the boundaries of the hole, they are also distributed throughout the domains at low densities. This behavior is typical of all films in the thickness range $L < h < 3L$ that we examined.

The smaller Au(2)-PS nanoparticles are distributed uniformly throughout the film, exhibiting no evidence of preferential segregation to the boundaries. This is apparent from the high-magnification image (Figure 1c) in which the boundary of hole is

visible, based on the contrast. In general, preferential segregation is only observed in BCP films containing nanoparticles sufficiently large in size and cannot be accommodated solely within the domains.

Further insight into the structure of the boundaries is provided in Figure 2. A STEM image of a film of average thickness $1.4L$, containing 3 wt % NPs, is shown in Figure 2a. The schematic of the distribution of nanoparticles is shown in Figure 2b; it reveals that the NP clusters reside at the core of an edge dislocation. In thin film BCPs, the chains that comprise the dislocation core undergo significant distortion, experiencing a reduction in conformational entropy, within the core in order to accommodate the transition from the islands or holes to the layer below.[28] When the nanoparticles are located within the core of the dislocation, the conformational entropy loss associated with chain stretching is minimized. This additional energy gain associated with the incorporation of the nanoparticles, of larger d/L, within the dislocation cores is greater than would be gained by incorporating them within the normal domain structure (Figures 2b2 and 2b1). It is noteworthy that studies of *bulk* BCP−nanoparticle systems reveal that the NPs preferentially segregate at tilt boundaries.[21,34] In light of this, our observation that nanoparticles of sufficient size would preferentially reside within the defects

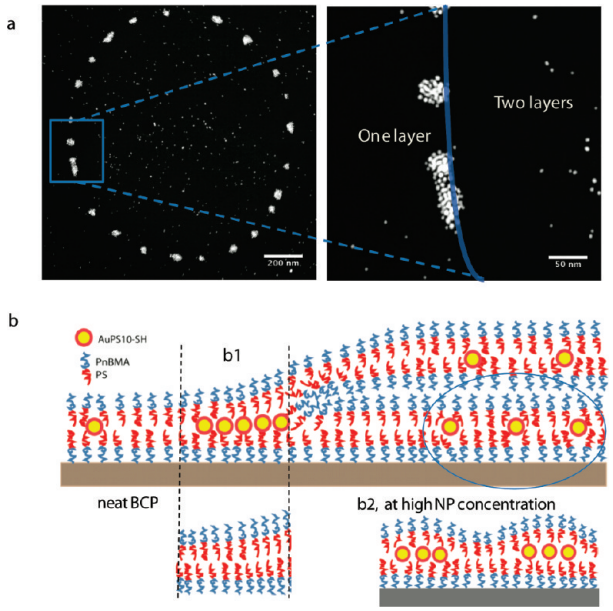

Figure 2. Preferential segregation of nanoparticles to the dislocation core surrounding an island. (a) STEM image of nanoparticle clusters at the perimeter of a island in a film of thickness $h = 1.4L$. (b) Schematic of the cross section of the film illustrating how the nanoparticles are located at the core of an edge dislocation (extra partial layer); (b2) a copolymer domain layer containing nanoparticles is shown to undergo a local elastic distortion to accommodate the nanoparticles.

should not be surprising. The segregation in both cases is due largely to entropic effects.

An assessment of the early time evolution of the nanoparticle distribution provides insight into the mechanism by which the final morphology of the BCP nanocomposite film develops. Initially after spin-casting the NPs are nearly uniformly distributed throughout the film, as shown by the STEM image (Figure 3a) of a film containing 3 wt % nanoparticles. The islands and holes do not exist during this early stage. Nanoparticle aggregates develop as the structure of the film approaches equilibrium, due to annealing (Figures 3b,c). Our observations are that while the islands (or holes) form concurrently with the segregation of nanoparticles to the dislocation cores, the development of the islands and holes is completed well in advance of the completion of the segregation process.

For samples containing larger NP concentrations, the average size of the NP clusters increases; additionally NP clusters reside throughout the domains. The lateral distribution of NPs is illustrated in Figure 4a for a sample containing 13 wt % nanoparticles; the average NP cluster size is larger than that of the 3 wt % samples. Unlike the 3 wt % samples, NP clusters reside throughout the domains, away from the boundaries. The existence of clusters away from the boundaries of the islands is particularly evident from the STEM image in Figure 4b and the SFM image in Figure 4c. A line profile from the SFM image (Figure 4d) indicates that regions away from the islands exhibit significant local elastic deformation to accommodate the nanoparticles. In fact, the increase in thickness locally is ~50% larger than the domain size.

The basic picture that emerges is the following. For the smallest values of d/L, the nanoparticles reside throughout the appropriate domains and maximize their translational entropy. However for sufficiently large d/L, the nanoparticles preferentially reside in the dislocation cores where it is entropically more favorable. Clearly, there is a partitioning of these larger nanoparticles between the dislocation cores and the normal domains, based on nanoparticle composition and size.

We now further examine the role of dislocations toward nanoparticle sequestration. For a sample of thickness $L < h < 2L$, an edge dislocation would necessarily reside in the vicinity of the free surface, stabilized by the surface tension. Turner et al. have shown that for a lamellar structure of n layers, in contact with a substrate, the total elastic energy of a single dislocation is approximated to be

$$F \approx (L/2)\gamma_{AB} + (L/2n^{1/2})(\gamma_{AB}\gamma) \qquad (1)$$

where γ is the surface tension of the component exposed to the free surface and $\gamma_{AB} \approx (KB)^{1/2}$; K and B are the bending and compression moduli, respectively.[29] This approximation assumes that the dislocation resides at its equilibrium location, near the center of the film. Note that the cost of placing an extra layer at the free surface (i.e., the edge dislocation) is proportional to the

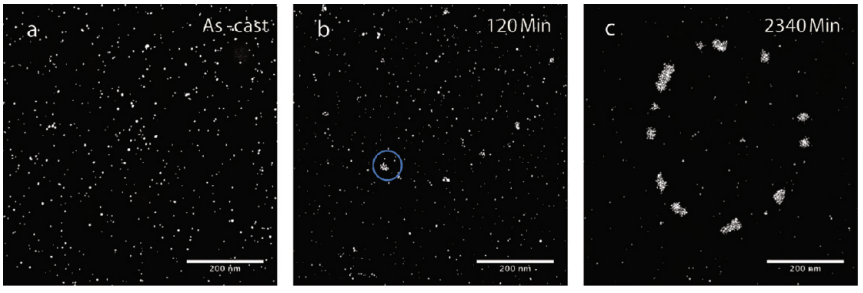

Figure 3. Structural evolution of a BCP film ($h = 1.4L$) is shown at different times: (a) as-cast; (b) time = 120 min; (c) time = 2340 min.

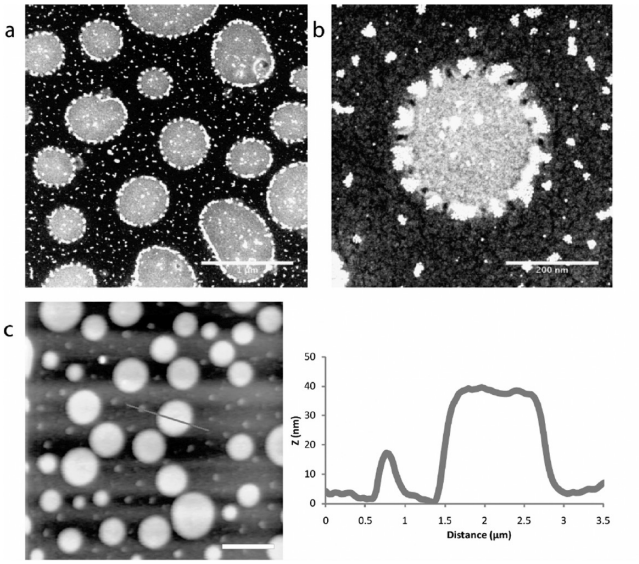

Figure 4. Lateral distribution of nanoparticles in film of thickness $h = 1.4L$, containing 13 wt % NPs. (a, b) STEM images. (c) SFM image. (d) A line scan showing the dimensions of an island as well as the local elastic deformation of the domain that develops to accommodate a nanoparticle cluster.

surface tension difference between the two components, $h\Delta\gamma$, whereas the cost for placing a dislocation below the free surface is $h\gamma_{AB}$. In the case of our copolymer system, PS-*b*-PnBMA, it has been shown that $\gamma_{AB} \sim 0.9$ dyn/cm and $\Delta\gamma \sim 9$ dyn/cm.[29] Therefore, the edge dislocation would reside beneath the surface. The "healing length", the length scale over which the boundary extends from the top of the island to the layer below (see Figure 5), is

$$\lambda \approx (\kappa H \Gamma)^{1/2} \tag{2}$$

where $\kappa = (K/B)^{1/2}$ and H is the total film thickness and $\Gamma = \gamma/(KB)^{1/2}$.[29] One of the key predictions of the theory is that λ should increase as the film thickness increases and the dislocation resides deeper into the film. The depth of the dislocation below the surface of the film is determined by $\Gamma = \gamma/(KB)^{1/2}$. It is evident from Figure 5a,b that λ is nearly twice as large for the thicker ($h = 5.7L$) sample. The data in Figure 5c indicate that the healing length in our system scales as in a manner consistent with $h^{1/2}$, in agreement with the theory as described above. This observation, $\lambda \propto h^{1/2}$, was first made in a study of pure PS-*b*-PnBMA systems by Turner et al.[29] While details of the theory remain unexplored, work by Lui et al. made it clear that dislocations would reside within the interior of thick BCP films.[36]

In the thinnest films, the healing length is smallest and the chains undergo more stretching than thicker films in order to accommodate the dislocation at the boundary of an island or hole. We note that when the film thickness increases the dislocation moves deeper within the film as suggested by the theory.[29] When the film thickness increases, the healing length increases; consequently, the chains evidently undergo less stretching to accommodate dislocation formation.

It would appear that this effect, the increasing λ and the associated relaxation of the chain stretching constraints, would influence the average size of the clusters. The images in Figure 6 indicate that the size of the aggregates of the nanoparticles are larger, on average, in the thicker $h = 5.7L$ film (Figure 6b) than in thinner $h = 2.7L$ film (Figure 6a). In Figure 6a, the average cluster size is relatively constant, 300 ± 60 nm^2, regardless of the size of the islands or hole, for a given concentration of nanoparticles. In the case of the $h = 5.7L$ film, the average cluster size is 1200 ± 400 nm^2. The schematic in Figure 5d provides an indication of the

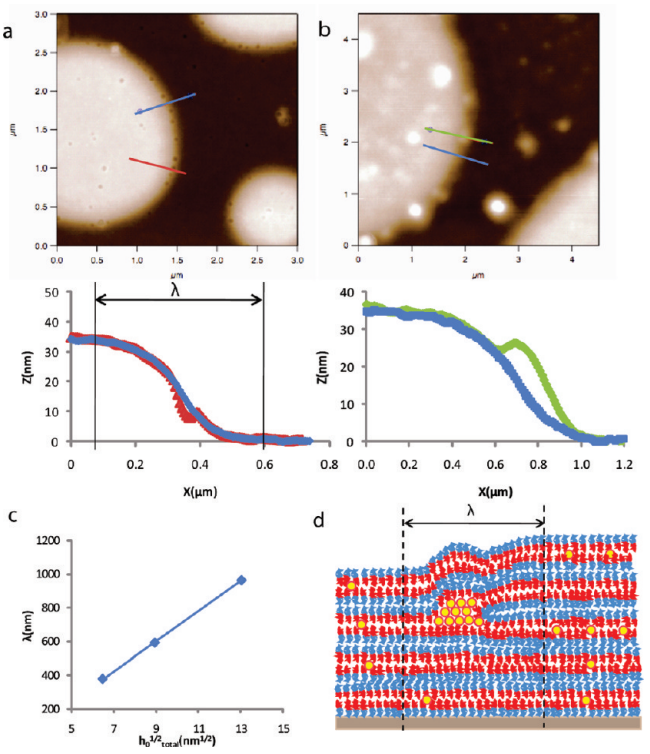

Figure 5. Images of islands and information about the healing lengths for films of different thicknesses (each sample contains 3 wt % nanoparticles). STEM images of typical islands on films of thicknesses (a) $h = 81$ nm $= 2.7L$ and (b) $h = 170$ nm $= 5.7L$. The corresponding line profiles at the edge of the islands are shown below each image in order to illustrate the magnitude of the "healing length", λ. The fluctuations in the shape of the lines are due to the presence of nanoparticles. (c) Healing length plotted as a function of $h^{1/2}$. (d) Schematic, constructed using information from SFM and STEM images, showing nanoparticles located in the core of an edge dislocation that lies a few layers below the surface of a film.

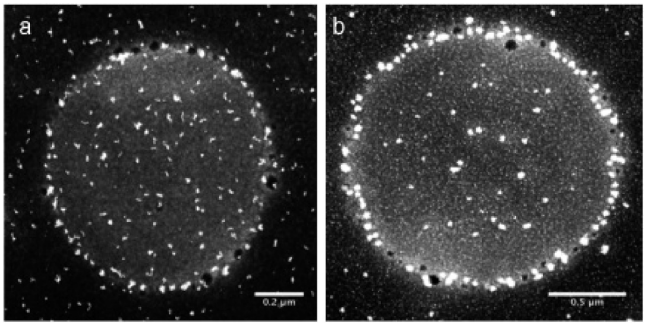

Figure 6. STEM images of NP clusters that form in films of different thicknesses: (a) $h = 81$ nm ($2.7L$) and (b) 170 nm ($5.7L$).

probable structure of this system when the film is thick; in this case the cluster is not 2-dimensional, as it is for the thin films of $h < 3L$.

It is noteworthy that the NPs are not uniformly distributed along the boundaries of the islands (or holes); instead, they form clusters, and the number of clusters per unit length along the perimeter is constant regardless of island size within the film (Figure 7). We speculate that the formation of clusters may be understood from the following. The chain grafting density of the nanoparticles and the grafting chain length are such that the PS components of the BCP that comprise the appropriate domains would not interpenetrate the grafted layers. We are confident of this fact as we have shown that these nanoparticles are immiscible to PS homopolymers of a wide range of molecular weights, as low as

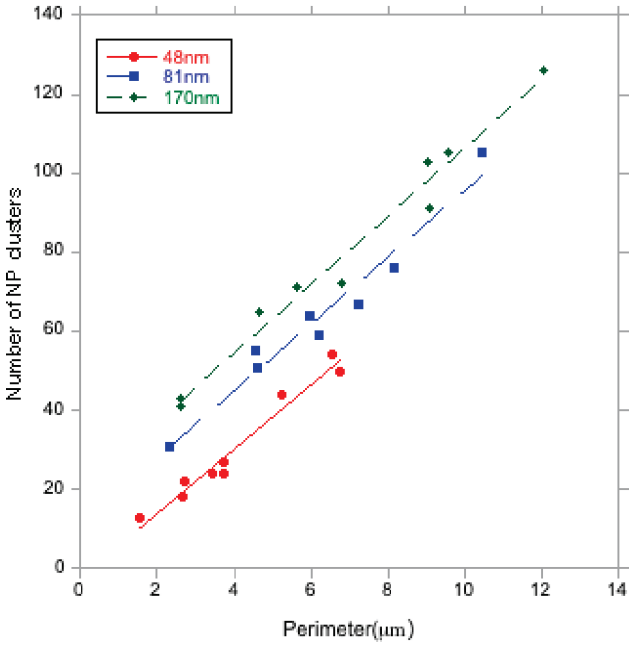

Figure 7. Distributions of NP clusters along the perimeters of edge dislocations in films of different thicknesses (each sample contains 3 wt % nanoparticles).

10 kg/mol. In the absence of interpenetration between the grafted and the PS copolymer chains, the nanoparticles show a tendency to cluster in order to minimize the area of contact between the copolymer layer and the nanoparticles. The energy cost is evidently minimized when the nanoparticles form clusters instead for residing uniformly throughout the domains. The fact that the cluster−cluster separation distance is relatively constant is consistent with the notion that the clusters reside within a single plane.

A future study examining the connection between core size, healing length, and the depth of the dislocation below the free surface is planned. Such a study would include thicker films, and it is possible to get cross-sectional TEM images showing the location of the dislocation below the free surface, enabling a direct comparison with additional predictions of the theory. We are currently examining the long-time structural of the evolution (i.e., coarsening phenomena) of the islands/holes, using the nanoparticles as markers.

Concluding Remarks

We showed that for BCP films that order at suboptimal thickness defects play a central role in the assembly of nanoparticles, provided d/L is sufficiently large. Specifically, a significant fraction of the nanoparticles reside at the core of edge dislocations. Consequently, the planar 2D geometry of the islands and holes dictates the pattern formation of the self-assembled nanoparticles. Of course, when d/L is very small, the nanoparticles tend to be located within the domains, thereby maximizing the translational entropy.

Our findings will impact the manner in which BCP thin films are used for nanofabrication. Future theoretical efforts should consider the role of defects and their impact on the free energy of the thin films in order to understand phase transitions and other structural phenomena in thin film BCPs systems containing large nanoparticles.

Acknowledgment. This work was supported by the US Department of Energy, Office of Science, Basic Energy Research (BES), Synthesis and Processing Program.

References and Notes

(1) Underhill, R. S.; Liu, G. *Chem. Mater.* **2000**, *12* (12), 3633–3641.
(2) Bockstaller, M.; Kolb, R.; Thomas, E. L. *Adv. Mater.* **2001**, *13* (23), 1783–1786.
(3) Coakley, K. M.; McGehee, M. D. *Chem. Mater.* **2004**, *16* (23), 4533–4542.
(4) Huynh, W. U.; Dittmer, J. J.; Alivisatos, A. P. *Science* **2002**, *295* (5564), 2425–2427.
(5) Bockstaller, M. R.; Mickiewicz, R. A.; Thomas, E. L. *Adv. Mater.* **2005**, *17* (11), 1331–1349.
(6) Haryono, A.; Binder, W. H. *Small* **2006**, *2* (5), 600–611.
(7) Kim, B. J.; Bang, J.; Hawker, C. J.; Kramer, E. J. *Macromolecules* **2006**, *39* (12), 4108–4114.
(8) Lee, J. Y.; Thompson, R. B.; Jasnow, D.; Balazs, A. C. *Macromolecules* **2002**, *35* (13), 4855–4858.
(9) Lee, J.-Y.; Thompson, R. B.; Jasnow, D.; Balazs, A. C. *Phys. Rev. Lett.* **2002**, *89* (15), 155503.
(10) Schultz, A. J.; Hall, C. K.; Genzer, J. *Macromolecules* **2005**, *38* (7), 3007–3016.
(11) Pryamitsyn, V.; Ganesan, V. *Macromolecules* **2006**, *39* (24), 8499–8510.
(12) Thompson, R.; Ginzburg, V.; Matsen, M.; Balazs, A. *Science* **2001**, *292* (5526), 2469.
(13) Kim, B. J.; Fredrickson, G. H.; Hawker, C. J.; Kramer, E. J. *Langmuir* **2007**, *23* (14), 7804–7809.
(14) Orso, K. A.; Green, P. F. *Macromolecules* **1999**, *32* (4), 1087–1092.
(15) Hamdoun, B.; Ausserré, D.; Cabuil, V.; Joly, S. *J. Phys. II* **1996**, *6* (4), 503–510.
(16) Listak, J.; Hakem, I. F.; Ryu, H. J.; Rangou, S.; Politakos, N.; Misichronis, K.; Avgeropoulos, A.; Bockstaller, M. R. *Macromolecules* **2009**, *42* (15), 5766–5773.
(17) Chiu, J. J.; Kim, B. J.; Kramer, E. J.; Pine, D. J. *J. Am. Chem. Soc.* **2005**, *127* (14), 5036–5037.
(18) Matsen, M. W.; Thompson, R. B. *Macromolecules* **2008**, *41* (5), 1853–1860.
(19) Gido, S.; Gunther, J.; Thomas, E.; Hoffman, D. *Macromolecules* **1993**, *26* (17), 4506–4520.
(20) Gido, S.; Thomas, E. *Macromolecules* **1994**, *27* (21), 6137–6144.
(21) Listak, J.; Bockstaller, M. *Macromolecules* **2006**, *39* (17), 5820–5825.
(22) Xu, C.; Ohno, K.; Ladmiral, V.; Milkie, D. E.; Kikkawa, J. M.; Composto, R. J. *Macromolecules* **2009**, *42* (4), 1219–1228.
(23) Bita, I.; Yang, J. K. W.; Jung, Y. S.; Ross, C. A.; Thomas, E. L.; Berggren, K. K. *Science* **2008**, *321* (5891), 939–943.
(24) Stoykovich, M.; Muller, M.; Kim, S.; Solak, H.; Edwards, E.; De Pablo, J.; Nealey, P. *Science* **2005**, *308* (5727), 1442.
(25) Kang, H.; Detcheverry, F.; Mangham, A.; Stoykovich, M.; Daoulas, K.; Hamers, R.; Müller, M.; de Pablo, J.; Nealey, P. *Phys. Rev. Lett.* **2008**, *100* (14), 148303.
(26) Park, S.; Lee, D. H.; Xu, J.; Kim, B.; Hong, S. W.; Jeong, U.; Xu, T.; Russell, T. P. *Science* **2009**, *323* (5917), 1030–1033.
(27) Green, P. F.; Limary, R. *Adv. Colloid Interface Sci.* **2001**, *94* (1−3), 53–81.
(28) Maaloum, M.; Ausserre, D.; Chatenay, D.; Coulon, G.; Gallot, Y. *Phys. Rev. Lett.* **1992**, *68* (10), 1575.
(29) Turner, M.; Maaloum, M.; Ausserré, D.; Joanny, J.; Kunz, M. *J. Phys. II* **1994**, No. 4, 689–702.
(30) Brust, M.; Walker, M.; Bethell, D.; Schiffrin, D.; Whyman, R. *J. Chem. Soc., Chem. Commun.* **1994**, *1994* (7), 801–802.
(31) Meli, L.; Li, Y.; Lim, K. T.; Johnston, K. P.; Green, P. F. *Macromolecules* **2007**, *40* (18), 6713–6720.
(32) Kim, J.; Green, P. F. *Macromolecules* **2010**, *43* (3), 1524–1529.
(33) Chen, X. C.; Green, P. F. *Langmuir* **2009**, *26* (5), 3659–3665.
(34) Thompson, R. B. *J. Chem. Phys.* **2010**, *133*, 144902.
(35) Lauter-Pasyuk, V.; et al. *Physica B* **1998**, *248*, 243–245.
(36) Liu, Y.; Rafailovich, M. H.; Sokolov, J. *Macromolecules* **1996**, *29* (3), 899–906.